Proceedings of IEEE SMARTGRIDCOMM 2014, Venice, Italy, November 3-6, 2014.

Statistical Analysis of Broadband Underground Medium Voltage Channels for PLC Applications

Fabio Versolatto*, Andrea M. Tonello*†, Carlo Tornelli‡, and Davide Della Giustina§
* WiTiKee Srl - Udine - Italy
e-mail: {versolatto, tonello}@witikee.com
† University of Udine - Udine - Italy
‡ RSE SpA -Milano - Italy
e-mail: carlo.tornelli@rse-web.it
§ A2A Reti Elettriche SpA - Brescia - Italy
e-mail: davide.dellagiustina@a2a.eu

***Abstract*—This work presents a statistical analysis performed on a set of channels that were measured in real-life underground medium voltage power line communication (PLC) networks. The aim is to improve the knowledge of the medium from experimental basis, providing usable and closed-form expressions of the main metrics in order to foster the design of PLC technologies tailored to such challenging scenario.**

The work targets the 2-40 MHz band, and focuses on the average channel gain (ACG), the root-mean-square delay spread (RMS-DS) and the coherence bandwidth. Furthermore, the work presents the relation between the ACG, the RMS-DS and the network topology, and it infers the capacity as a function of the transmission bandwidth under power spectral density or total power constraints. Some results about the line impedance are also shown.

I. Introduction

Power line communications (PLC) has gained a prominent role in the smart grid context, as a valuable solution for communications over the power cables. In particular, PLC has proved to be suitable for a multitude of applications, as automatic meter reading or remote control, and it can be deployed both on low and medium voltage networks.

This work focuses on the medium voltage (MV) part of the distribution network and it targets underground installations. Underground MV networks were formerly studied in [1]-[2]. In detail, [1] presents an analytical model of the propagation on underground cables, [3] deepens the study in terms of capacity and highlights that even though the underground lines are characterized by a disruptive attenuation, they can compete with overhead lines because the experienced noise is lower and the transmit power limit is higher. Field trials performed by Ofcom reveal that a power spectral density (PSD) level of -40 dBm/Hz in the band 1.705-30 MHz and of -57 dBm/Hz in the band 30 - 88 MHz are appropriate to ensure compliance with the limits defined by the FCC part 15 [3]. These limits are 20 dB larger than those that apply for the overhead lines. Finally, [2] provides an analysis in terms of scattering parameters. A theoretical model of MV channels based on the transmission-line theory is presented in [4] and it is validated by an in-depth analysis of the simulated results.

The former works do not address the experimental statistics of some relevant metrics ([4] deals mainly with simulated quantities), as the average channel gain (ACG), the root-mean-square delay spread (RMS-DS) or the coherence bandwidth (CB), that are fundamental for the design of the PLC transmission scheme. For instance, the optimal cyclic prefix and the number of sub-carriers of a multi-carrier modulation scheme can be obtained from the RMS-DS and the CB, respectively.

In this respect, herein, a study on the statistics of the ACG, RMS-DS and CB of a set of channels measured in two real-life underground MV Italian networks is presented. Further, the correlation between the metrics and the topology, some new results about the capacity and a preliminary study on the line impedance are presented. The results, in conjunction with those from prior measurement campaigns, as [5], are important to get a thorough insight on an incredibly heterogeneous PLC scenario as the underground MV one.

The statistics of the metrics have been obtained exploiting Channel Manager, a Matlab-based GUI-enabled software developed by WiTiKee for the smart management of large databases. The software is a full-custom solution that processes the files generated by instruments, to obtain the statistics of the most relevant metrics in a graphical form.

The remainder of the work is as follows. Section II presents the measurement setup, the measurement sites and the post-processing performed on the measures. Section III deals with the statistics of the channel response in terms of the main metrics and the relation between the topology and the channel statistics. Then, Sections IV-V provide the results of the capacity analysis and the line impedance, respectively. Finally, some conclusions follow.

II. Measurements and Post-Processing

The statistical analysis presented in Section III is carried out on a set of measured channels acquired in two different real-

This work was partly funded by the Research Fund for the Italian Electrical System under the Contract Agreement between RSE SpA and the Ministry of Economic Development - General Directorate for Nuclear Energy, Renewable Energy and Energy Efficiency in compliance with the Decree of Mar. 8, 2006.

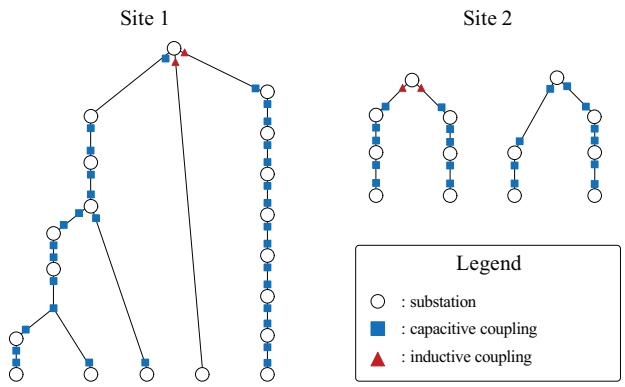

Fig. 1. Graph of the measurement sites. The coupler position is also shown.

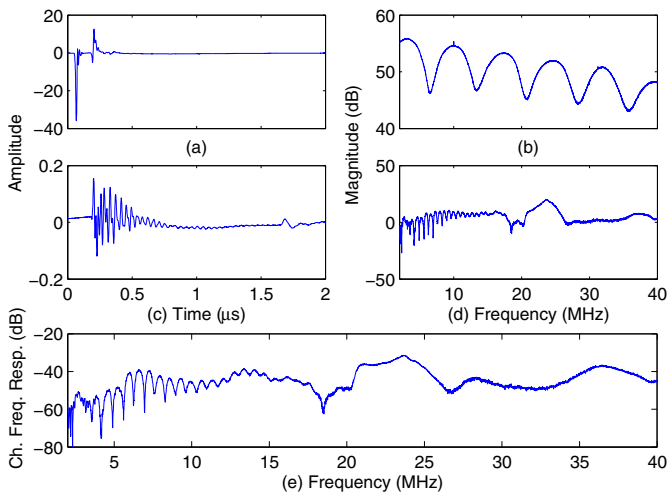

Fig. 2. On top, impulse (a) and frequency (b) response of the transmitted pulse. On the middle, impulse (c) and frequency (d) response of the received pulse. On bottom, channel frequency response example (e).

life underground MV networks. A time-domain measurement setup has been adopted as it provides an efficient solution to get the magnitude of the channel response.

A. Description of the Measurement Sites

Measurements were performed in two underground MV power delivery networks in Italy. We denote the networks as site 1 (S1) and site 2 (S2). The networks consist of multiple substations interconnected by underground MV cables. In the substations, medium to low voltage transformers are present. Fig. 1 shows the graph of the network structure of both sites. S1 exhibits a tree like structure with few branches. S2 shows a linear structure and it is made of two sub-networks.

In S1, the length of the cables varies from 64 m to 1002 m, with a mean value of approximately 476 m. In S2, the length of the cables is comprised between 82 and 694 m, with a mean value of approximately 334 m. Some further topological details are available for S1. In particular, the cables that interconnect subsequent stations are made of different trunks with no derivations, but in general with cables of different types. The number of trunks varies from one, i.e., direct end-to-end connection between the substations, up to five. The length of the trunks varies from 4 m up to 635 m.

Broadband capacitive couplers are installed in most of the substations and they are connected in correspondence of the termination ends of the underground MV cables. Four additional inductive couplers are deployed. The couplers show a pass-band between $f_i = 2$ MHz and $f_e = 40$ MHz, an input impedance of 50 Ω on the equipment side, and of 20 Ω on the line side.

B. Measurement Setup

Channel measurements were performed in the time domain with a pulser at the transmitter side and a digital storage oscilloscope (DSO) at the receiver side. The pulser was deployed in combination with a linear amplifier. The transmitted pulse was acquired connecting the DSO to the output port of the amplifier, with a high input impedance. At the receiver side, the DSO was deployed to acquire the received signal and it was configured to show an input impedance of 50 Ω.

Fig. 2 shows the impulse and frequency response of an example of transmitted and received pulse, and the correspondent channel frequency response computed as described in Section II-C. Frequency plots are limited to the pass-band of the capacitive couplers.

The DSO was configured to acquire a time window of 10 ms, with a sampling period T_s of 1 ns. The actual measurement is averaged over subsequent acquisitions to limit the effect of noise impairments. Furthermore, the DSO was triggered to detect the transmitted pulse, with an appropriate trigger level.

C. Post Processing

The channel frequency response can be obtained from the transmitted and received signal. Let us denote with $v_x(t)$, $x \in \{T, R\}$, the transmitted (T) and received (R) waveform, respectively, where we adopt a continuous time-domain notation for simplicity. The correspondent Fourier transforms read $V_x(f) = \mathcal{F}\left[v_x(t)\right](f)$, $x \in \{T, R\}$, where $\mathcal{F}[\cdot]$ denotes the Fourier transform operator. Hence, the channel frequency response is given by $H(f) = V_R(f)/V_T(f)$. Clearly, the former relation is meaningful in the range of frequencies for which the spectrum components of $V_R(f)$ exceed the noise. In this respect, to enable the comparison with prior works [5], we limit the study herein presented on the pass-band frequency of the capacitive couplers, i.e., 2-40 MHz. Furthermore, we compute the impulse response from $H(f)$ as described in [6] and as implemented in the Matlab script that we have made available online in [7]. Basically, we compute the inverse-Fourier transform, and we cut the tails of the impulse response to keep the 98% of the channel energy.

III. Statistical Analysis

The aim of this Section is to provide some results on the statistics of the measured channels and to enable the comparison with the results of other measurement campaigns presented in prior works in the literature.

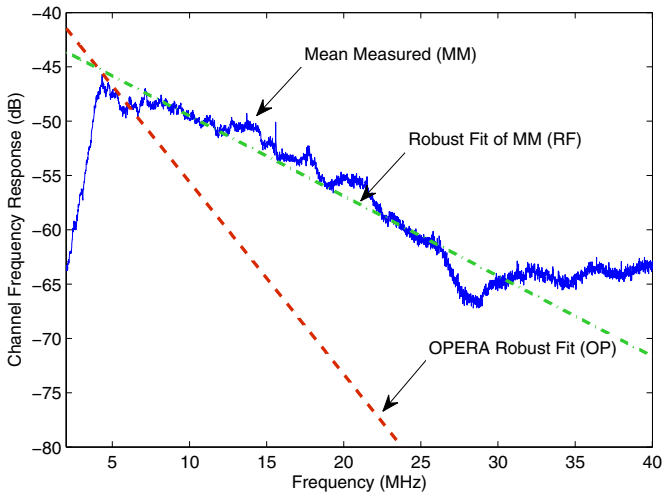

Fig. 3. Mean of the measured channels (MM) in dB, its robust fit (RF) and robust fit of the MV channels reported in [8] (OP).

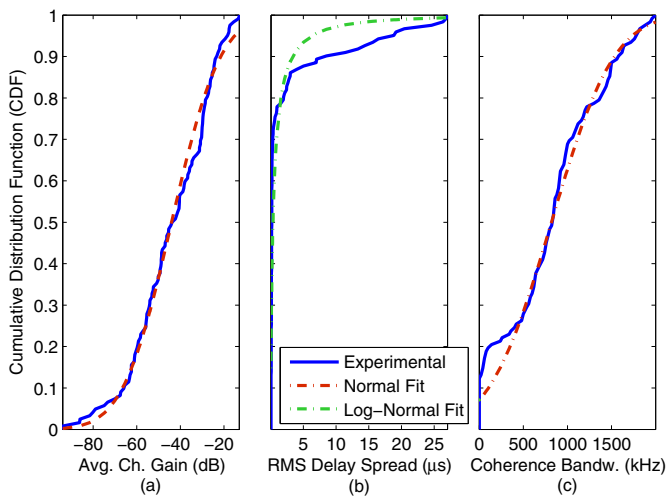

Fig. 4. Cumulative distribution function of the average channel gain (a), the root-mean-square delay spread (b), and the coherence bandwidth (c).

A. Channel Frequency Response

The measured channels exhibit an average attenuation that is significantly lower than that reported by prior works in the literature. Fig. 3 shows the mean of the measured channel responses in dB (measured mean, MM), i.e., $P(f) = 20\log_{10}\left(E\left[|H(f)|\right]\right)$ where $E\left[\cdot\right]$ denotes the expectation over measurements, its robust fit (RF), and the robust fit of the measured channel responses in dB scale reported in [8] (OP). RF reads

$$P(f) = -0.749 \cdot 10^{-6} f - 42.1 \quad [\text{dB}], \tag{1}$$

while OP is described analytically as follows

$$P(f) = -1.77 \cdot 10^{-6} f - 37.9 \quad [\text{dB}]. \tag{2}$$

We speculate that the small attenuation highlighted by RF is a consequence of the differences in the channel backbone length, that is, on average, equal to 345 m for the channels herein considered, and to 500 m for the channels in [8]. Beside the attenuation differences, we note the following. Firstly, MM exhibits a large attenuation below 5 MHz that reflects the high-pass behavior of the couplers. Similar results were pointed out in [9]. Secondly, MM flattens above 30 MHz because, we speculate, the limited sensibility of the DSO does not enable evaluating the extremely high attenuations.

B. Statistical Metrics

We now focus on the ACG, the RMS-DS, and the CB [6]. Basically, the ACG provides an indication about the mean frequency attenuation of the channel, the RMS-DS describes the channel time dispersion, and the CB quantifies the frequency selectivity. We compute the metrics as described in [6], where we refer for further details. Fig. 4 shows the cumulative distribution function (CDF) of the ACG, RMS-DS and the CB of the measured channels. The ACG is comprised in the range between -70 and -10 dB, with a mean value of -44.13 dB, and it is distributed as a normal variable with good approximation. These results confirm the ones reported in the literature, e.g., [5]. Indeed, the RMS-DS exhibits some strong deviations from the log-normal distribution, i.e., its best fit according to the literature, e.g., [5]. This result can be motivated by the presence of outliers with extremely high delay spread values, say, in the order of some tens of μs. In general, more than 70% of the channels exhibit an RMS-DS lower than 1 μs. Finally, the CB is normally distributed with good approximation and it is lower than 1.3 MHz in 80% of the cases. Some deviations from the normal distribution can be observed for the lowest CB values.

Now, let us further investigate the relation between the metrics. Fig. 5(a)-(b) show the relation between the ACG and the RMS-DS, and between the RMS-DS and the CB. The former plot is limited to the RMS-DS values below 5 μs to magnify the range of the most representative channels. As it can be noted, the robust regression fit ranges from 0.1 to 0.27 μs. In particular, the robust regression fit reads

$$\sigma_\tau = -0.0023G + 0.062 \quad [\mu\text{s}], \tag{3}$$

where σ_τ denotes the RMS-DS in μs and G is the ACG in dB. In [5], a similar study on another set of underground MV channels pointed out a slope of -0.0075 μs/dB and an intercept of 0.183 μs. Hence, the channels herein described are less spread in time though the attenuation values are similar. In the in-home scenario, the same relation holds and the slope reads 0.0085 μs/dB [6].

Indeed, the relation between the RMS-DS and the CB can be fitted by the following hyperbolic line

$$B = \frac{167.2}{\sigma_\tau} \quad [\text{kHz}]. \tag{4}$$

This result is similar to that of the in-home scenario, e.g., [6], where, however, the constant coefficient in (4) reads 57 kHz/μs, i.e., given a RMS-DS value, the in-home channel

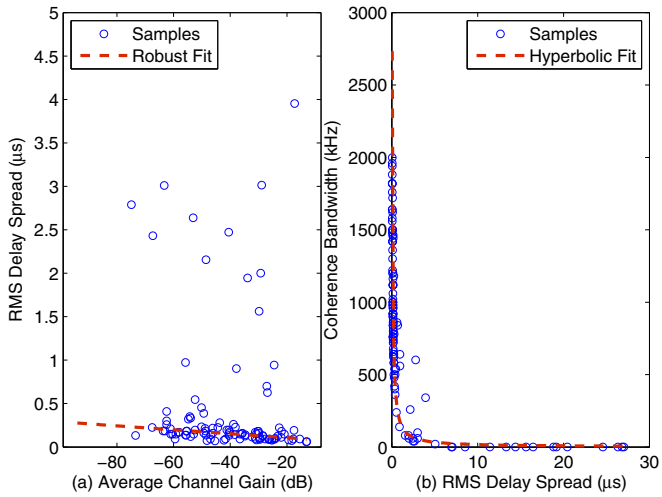

Fig. 5. On the left, RMS-DS versus ACG. On the right, CB versus RMS-DS. In both the cases, the best fit is also shown.

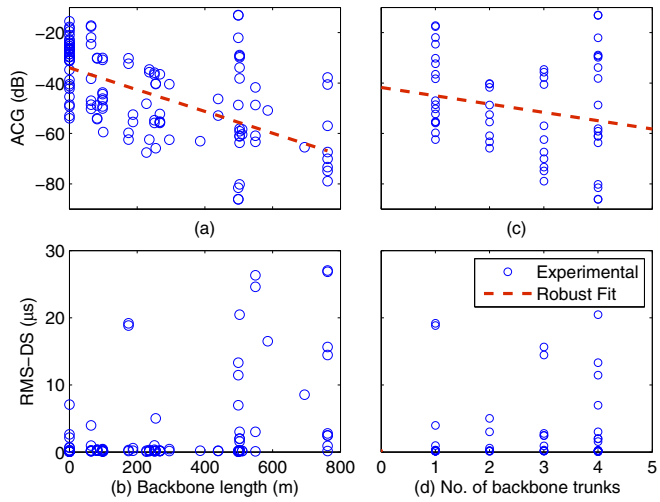

Fig. 6. ACG and RMS-DS as a function of the backbone length (a)-(b), and of the number trunks (c)-(d). For the ACG, the robust fit is also shown.

exhibits severe frequency fading. However, note that [6] is focused on the extended frequency band up to 100 MHz.

C. Topology Correlation

We herein aim to infer the relation between the channel statistics and the underlying topology. This study is limited to one of the two sites, for which all the topological information is available. We focus on the metrics of Section III-B and we relate them to the backbone length and the number of backbone trunks. The measurements have been performed between subsequent stations. The stations are connected by MV links. The length of the MV links is the backbone length. Each MV link is made by up to five cable (backbone) trunks. In general, the trunks are homogeneous, but the interconnection of subsequent trunks leads to reflections.

Fig. 6 shows the results. The backbone length is considered zero for the channels measured between couplers within the same substation. From the figures, we note the following.

- The ACG decreases as the backbone length increases (see Fig. 6(a)), and the slope is quantified in -0.0432 dB/m.
- The channels within the same substation, i.e., with a null backbone length exhibit a quite spread ACG, from -20 to -60 dB. This result needs to be further investigated, and related to the characteristics of the substation, as the number of departing lines, the type of the line breakers, the coupler installation, etc..
- The largest RMS-DS values are associated to the longest channels, i.e., the RMS-DS spread increases with the backbone length (see Fig. 6(b)).
- The ACG decreases as the number of trunks increases with a slope of -3.28 dB/n, where n is the number of trunks. However, this is a mean trend because, for instance, the channels with four trunks exhibit a lower attenuation in contrast to the robust regression fit.
- No clear connection between the RMS-DS and the number of trunks can be evidenced from the study of Fig. 6(d). This result is surprising and need to be further investigated because intuition suggests that the time-dispersion due to reflections should increase with the number of discontinuities (trunks).

IV. Capacity Analysis

We now analyze the channel capacity assuming the noise to be additive colored Gaussian and the transmitted power spectral density to be -40 dBm/Hz in the frequency band 2 - 30 MHz, and -60 dBm/Hz beyond 30 MHz, according to the recommendations made in [3]. In this first study, we neglect the role of the impulsive noise, and we compute the capacity as

$$C = \int_{f_1}^{f_2} \log_2 \left(1 + \frac{|H(f)|^2 P_t(f)}{P_n(f)} \right) df \quad [\text{bps}], \qquad (5)$$

where f_1, f_2, $P_t(f)$, $P_n(f)$ are the start and the stop signaling frequency, the transmitted PSD, and the noise PSD, respectively. We obtain the noise PSD from measurements. More details can be found in Section IV-A. Finally, we propose a sub-band and a total power-constrained capacity study.

A. Background Noise

Underground MV noise traces were measured in the time-domain for all the receiver access points of site S1. The measures are representative of the worst-case noise scenario. From the time-domain traces, the noise PSD is obtained by means of Fourier transform (periodogram) and frequency-domain averaging. Fig. 7 shows the results. In most of the cases, the noise PSD exhibits a frequency decreasing profile, though some outliers exist. Fitting the measures, we obtain

$$P_n(f) = af^b + c \quad [\text{dBm/Hz}], \qquad (6)$$

where $a = -1.011 \cdot 10^{-7}$ dBm/Hz^2, $b = 1.09$ and $c = -110$ dBm/Hz. Namely, the fit is quasi-linear as b is close to the unit. In the following analysis, we compute the capacity of

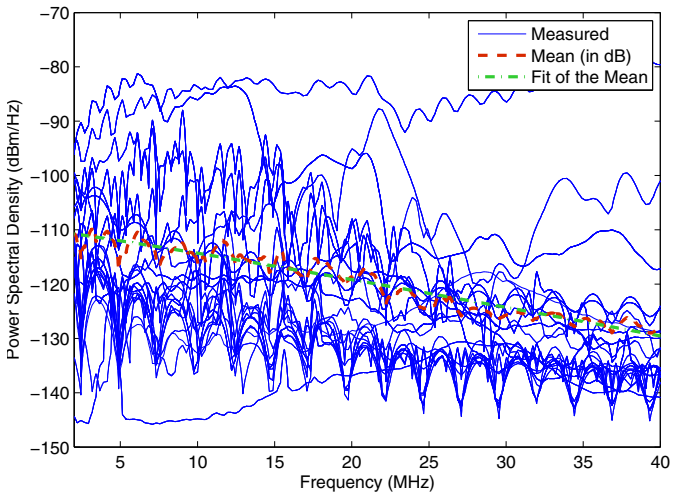

Fig. 7. Power spectral density profile of the noise obtained from the measured traces in the time domain.

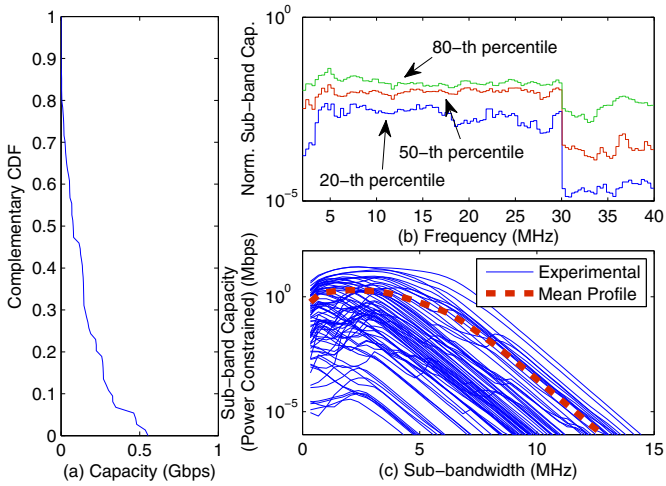

Fig. 8. C-CDF of the capacity computed in the band 2-40 MHz (a), 20-th, 50-th and 80-th quantiles of the normalized sub-band capacity (b), and capacity increasing the signaling bandwidth under a total power constraint (c).

the measured links substituting $P_n(f)$ in (5) with the actual noise PSD that was measured at the correspondent receiver port (not the mean profile in (6)).

B. Sub-band Capacity Analysis

Fig. 8(a) shows the complementary-cumulative distribution function (C-CDF) of the capacity of the measured channels that we compute as in (5) with $f_1 = f_i$ and $f_2 = f_e$. From the figure, datarates of up to 600 Mbps are possible under the worst-case noise assumption (see Section IV-A). Furthermore, in 80% of the cases, the capacity exceeds 10 Mbps.

Now, we consider the narrowband PLC technology that, according to FCC, can occupy the spectrum 145-478 kHz. We are interested in investigating whether its application to higher frequencies may provide some benefit. In the smart grid, narrowband PLC is commonly deployed for metering applications in the outdoor low voltage scenario. Its extensive usage in the MV grid is impeded by medium to low voltage transformers and repeaters are needed to bypass them. On the MV side, capacitive couplers can be deployed. They often exhibit a high-pass behavior that attenuates the narrowband PLC signal. Thus, an idea that we propose is to perform a frequency up-conversion at the repeaters to exploit a different range of frequencies where the couplers and the channel exhibit lower attenuation and more benign behavior.

To provide an analysis of the potential advantage, we divide the 2-40 MHz spectrum into band portions B = 342.2 kHz, i.e., the FCC band [10], we denote the capacity of the k-th band portion with $C^{(k)}$ and we compute $C^{(k)}$ as in (5), where $f_1 = f_i + kB$, $f_2 = f_i + (k+1)B$, $k = 0, \ldots \mathcal{K}$, and $\mathcal{K} = \lfloor (f_e - f_i)/B \rfloor - 1$. We normalize $C^{(k)}$ to the channel capacity on the entire spectrum to obtain $\overline{C}^{(k)}$, namely,

$$\sum_{k=0}^{\mathcal{K}} \overline{C}^{(k)} = 1. \tag{7}$$

Fig. 8(b) reports the 20-th, 50-th and 80-th percentile of $\overline{C}^{(k)}$ for each band portion k as piecewise continuous lines. On average, between 5 and 30 MHz, all the sub-bands exhibit similar performance, while the abrupt variation at 30 MHz is due to the variation on the transmitted PSD. The best performance is achieved for sub-bands around 5 MHz.

Finally, we perform a total power-constraint analysis of the channel capacity to understand whether the use of larger bandwidths may provide some benefit, given that the total transmitted power is constant. We let the power to be that transmitted in a sub-band as described in Section IV-B, with a PSD of -40 dBm/Hz, and we compute the capacity as in (5) where $f_1 = f_i$ and $f_2 = f_i + (k+1)B$. Note that, in this case, the sub-bands are always defined starting from f_i.

Fig. 8(c) shows the results. The sub-band capacity exhibits a concave behavior for most of the channels and it is confirmed by the mean profile. We speculate that this behavior is due to the large attenuation experienced below 5 MHz, and the increasing channel attenuation at higher frequencies. From the mean capacity profile, the best choice, i.e., the capacity peak, is for a transmission sub-bandwidth of about 5 MHz. Beyond this limit, we observe a significant decrease of performance.

V. Line Impedance Analysis

The line impedance is studied herein. We refer to the line impedance, namely, $Z_i(f)$, as the load that is seen by the transmitter modem, or, equivalently, the input impedance exhibited by the MV coupler connected to the network. The actual nature of the line impedance is important for the design of the analog front-end (AFE) of the transmitter, and further, to avoid the bands where it falls to extremely low values that can be interpreted as a short-circuit and that may damage the AFE. We compute the line impedance as follows

$$Z_i(f) = \frac{V_T(f) Z_g(f)}{V_g(f) - V_T(f)} \quad [\Omega], \tag{8}$$

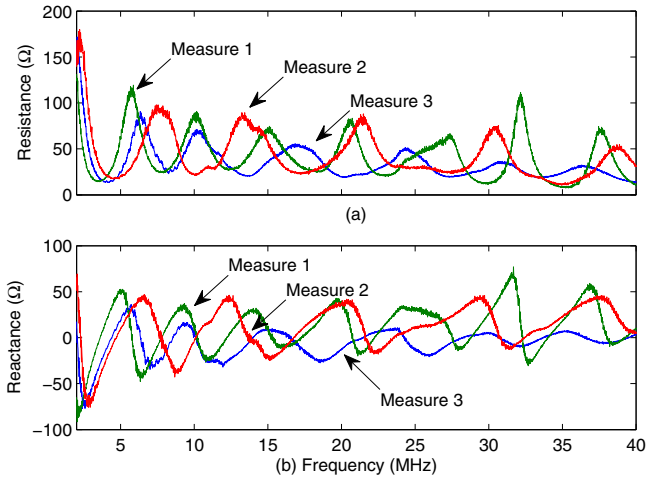

Fig. 9. Real part (on top) and imaginary part (on bottom) of three representative line impedances.

where $V_T(f)$, $V_g(f)$ and $Z_g(f)$ are the transmitted pulse as described in Section II-C, the ideal transmitted pulse and the internal impedance of the pulser, respectively. In (8), we explicit the frequency dependency of all quantities. Basically, we model the pulser as the series of the ideal voltage source $V_g(f)$ and the internal impedance $Z_g(f)$, and we obtain $V_g(f)$ as twice the waveform measured on a reference load equal to the internal impedance of the pulser, namely, $Z_g(f) = 50\,\Omega$. The latter quantity is measured configuring the DSO as described in Section II-C, for the transmitted pulse.

Fig. 9 shows the real and imaginary part of the line impedance of some representative measures. Most of the measures perform similarly to those in the figure, and they reproduce the impedance of a long transmission line (cable) closed into an unmatched load, as pointed out in [11]. Strictly,

$$Z_i(f) = Z_0 \frac{(1+\rho_L(f)) + (1-\rho_L(f))\tanh(\gamma(f)\ell)}{(1-\rho_L(f)) + (1+\rho_L(f))\tanh(\gamma(f)\ell)}, \quad (9)$$

where Z_0, $\gamma(f)$ and ℓ are the characteristic impedance, the propagation constant and the length of the cable, respectively. Furthermore, $\rho_L(f)$ is the reflection coefficient at the receiver side. For simplicity, we assume the characteristic impedance to be constant in frequency. From (9), it can be noted that with no reflections, i.e., $\rho_L(f) = 0$, the input impedance matches $Z_i(f) = Z_0$. Conversely, in the case of maximum reflections, i.e., $|\rho_L| = 1$, $Z_i(f)$ is dominated by the hyperbolic tangent and it performs as in Fig. 9.

Basically, the measured line impedances exhibit subsequent peaks and notches that are equally spaced in frequency and that correspond to zero-phase values. The real part ranges between few Ohms to 200 Ω and it is more spread at lower frequencies.

VI. Conclusions

A statistical characterization of underground MV channels has been presented from the results of an experimental measurement campaign that has been carried out in two real-life sites in Italy. The analysis has been focused on the channel frequency response, the average channel gain (ACG), the root-mean-square delay spread (RMS-DS), the coherence bandwidth (CB) and the channel capacity, and the results are representative of underground MV networks of densely populated areas.

In detail, the mean channel frequency response has been fitted, and the result has been compared to that of a previous measurement campaign in the literature. A lower mean attenuation of the measured channels has been found. It may be amenable to a lower length of the considered links.

The ACG, RMS-DS, and CB have been studied in terms of their CDF. Furthermore, the relation between the ACG and the RMS-DS and between the RMS-DS and the CB have been pointed out and compared to that in the literature. The statistics of the ACG and the RMS-DS have been also related to some characteristics of the topology, i.e., the backbone length and the number of backbone trunks. The capacity has been inferred both considering the whole signaling spectrum or dividing the spectrum into sub-bands. Furthermore, a study of the capacity under a total power constraint has been presented.

Finally, some results about the frequency behavior of the line impedance have been presented.

References

[1] A. G. Lazaropoulos and P. G. Cottis, "Broadband Transmission via Underground Medium-Voltage Power Lines – Part I: Transmission Characteristics," *IEEE Trans. Power Del.*, vol. 25, no. 4, pp. 2414–2424, October 2010.

[2] R. Aquilué, M. Ribó, J. R. Regué, J. L. Pijoan, and G. Sánchez, "Scattering Parameters-Based Channel Characterization and Modeling for Underground Medium-Voltage Power-Line Communications," *IEEE Trans. Power Del.*, vol. 24, no. 3, pp. 1122–1131, July 2009.

[3] A. G. Lazaropoulos and P. G. Cottis, "Broadband Transmission via Underground Medium Voltage Power Lines – Part II: Capacity," *IEEE Trans. Power Del.*, vol. 25, no. 4, pp. 2425–2434, October 2010.

[4] A. G. Lazaropoulos, "Towards Modal Integration of Overhead and Underground Low-Voltage and Medium-Voltage Power Line Communication Channels in the Smart Grid Landscape: Model Expansion, Broadband Signal Transmission Characteristics, and Statistical Performance Metrics," *Hindawi ISRN Signal Proc.*, vol. 2012, 2012.

[5] S. Galli, "A Novel Approach to the Statistical Modeling of Wireline Channels," *IEEE Trans. Commun.*, vol. 59, no. 5, pp. 1332–1345, May 2011.

[6] A. M. Tonello, F. Versolatto, and A. Pittolo, "In-Home Power Line Communication Channel: Statistical Characterization," *IEEE Trans. Commun.*, vol. 62, no. 6, pp. 2096–2106, Jun. 2014.

[7] From the PLC Channel Measurements to the Statistics: A Matlab Script. [Online]. Available: www.diegm.uniud.it/tonello

[8] M. Babic et al., "OPERA Deliverable D5. Pathloss as a Function of Frequency, Distance and Network Topology for Various LV and MV European Powerline Networks," OPERA-IST Integrated Project No 507667, 2005.

[9] S. Tsuzuki, T. Takamatsu, H. Nishio, and Y. Yamada, "An Estimation Method of the Transfer Function of Indoor Power-line Channels for Japanese Houses," in *Proc. IEEE Int. Symp. Power Line Commun. and Its App. (ISPLC)*, Mar. 2002, pp. 55–59.

[10] L. D. Bert, S. D'Alessandro, and A. M. Tonello, "A G3-PLC Simulator for Access Networks," in *Proc. Int. Symp. on Power Line Commun. and Its App. (ISPLC)*, March 2014, pp. 99–104.

[11] M. Antoniali and A. M. Tonello, "Measurement and Characterization of Load Impedances in Home Power Line Grids," *IEEE Trans. Instrum. Meas.*, vol. 63, pp. 548–556, Mar. 2014.